

Article

Metal Hydride Hydrogen Storage (Compression) Units Operating at Near-Atmospheric Pressure of the Feed H₂

Boris Tarasov ^{1,2}, Artem Arbuzov ¹ , Sergey Mozhzhukhin ¹, Aleksey Volodin ¹, Pavel Fursikov ¹, Moegamat Wafeeq Davids ³, Joshua Adeniran ³  and Mykhaylo Lototskyy ^{1,3,*} 

¹ Federal Research Center of Problems of Chemical Physics and Medicinal Chemistry, Russian Academy of Sciences (FRC PCP&MC RAS), Ac. Semenov Av. 1, Chernogolovka 142432, Russia; tarasov@icp.ac.ru (B.T.)

² Higher School of Economy, National Research University, Moscow 101000, Russia

³ HySA Systems Centre of Competence, University of the Western Cape, Robert Sobukwe Rd., Bellville 7535, South Africa

* Correspondence: mlototskyy@uwc.ac.za

Abstract: Metal hydride (MH) hydrogen storage and compression systems with near-atmospheric H₂ suction pressure are necessary for the utilization of the low-pressure H₂ produced by solid oxide electrolyzers or released as a byproduct of chemical industries. Such systems should provide reasonably high productivity in the modes of both charge (H₂ absorption at $P_L \leq 1$ atm) and discharge (H₂ desorption at $P_H = 2\text{--}5$ atm), which implies the provision of H₂ equilibrium pressures $P_{eq} < P_L$ at the available cooling temperature ($T_L = 15\text{--}20$ °C) and, at the same time, $P_{eq} > P_H$ when heated to $T_H = 90\text{--}150$ °C. This work presents results of the development of such systems based on AB₅-type intermetallics characterized by P_{eq} of 0.1–0.3 atm and 3–8 atm for H₂ absorption at $T_L = 15$ °C and H₂ desorption at $T_H = 100$ °C, respectively. The MH powders mixed with 1 wt.% of Ni-doped graphene-like material or expanded natural graphite for the improvement of H₂ charge dynamics were loaded in a cylindrical container equipped with internal and external heat exchangers. The developed units with a capacity of about 1 Nm³ H₂ were shown to exhibit H₂ flow rates above 10 NL/min during H₂ charge at ≤ 1 atm when cooled to ≤ 20 °C with cold water and H₂ release at a pressure above 2 and 5 atm when heated to 90 and 120 °C with hot water and steam, respectively.

Keywords: metal hydrides; AB₅; hydrogen storage and compression; low-pressure hydrogen



Citation: Tarasov, B.; Arbuzov, A.; Mozhzhukhin, S.; Volodin, A.; Fursikov, P.; Davids, M.W.; Adeniran, J.; Lototskyy, M. Metal Hydride Hydrogen Storage (Compression) Units Operating at Near-Atmospheric Pressure of the Feed H₂. *Inorganics* **2023**, *11*, 290. <https://doi.org/10.3390/inorganics11070290>

Academic Editor: Hai-Wen Li

Received: 2 June 2023

Revised: 28 June 2023

Accepted: 4 July 2023

Published: 6 July 2023



Copyright: © 2023 by the authors. Licensee MDPI, Basel, Switzerland. This article is an open access article distributed under the terms and conditions of the Creative Commons Attribution (CC BY) license (<https://creativecommons.org/licenses/by/4.0/>).

1. Introduction

High-temperature steam electrolysis, primarily based on solid oxide cells (SOCs), is a promising method of hydrogen production [1]. However, due to technical difficulties related to cell sealing, almost all commercial SOCs operate at near-atmospheric pressures. In doing so, the generated hydrogen releases at $P \sim 1$ atm (absolute), thus requiring further compression. Similar near-atmospheric pressures are typical for hydrogen byproducts released in vast amounts by several chemical industries. For example, the hydrogen production capacity of chlor-alkali plants in the U.S.A. ranges from 20 to 100 thousand tons annually [2], and the utilization of this hydrogen could bring significant benefits. At the same time, the minimum input/suction pressure of conventional mechanical hydrogen compressors does not typically exceed 4–5 atm [3]. Thus, it will be promising to collect low-pressure H₂ in a metal hydride (MH) and to further deliver it at a higher pressure using thermally driven compression [4].

An obvious material solution to realize this approach is the use of hydride-forming material characterized by hydrogen equilibrium pressure (P_{eq}) below 1 atm when absorbing the feed H₂. However, the challenge will be in providing reasonably high productivities in both charge (H₂ absorption) and discharge (H₂ desorption) modes. Indeed, maximizing the pressure driving force for H₂ absorption requires the values of P_{eq} to be close to zero. Such MH materials (hydrogen getters) are well known [5]. However, hydrogen release from the

H-saturated getter, even at low pressures requires too high temperatures, up to 650 °C [6]. At the same time, for the target application, the MH should provide sufficiently high H₂ discharge pressure (at least the 2–5 atm necessary for the suction in the next compression stage) when heated up to a moderate temperature, from 70 to 90 °C (provided by solar collectors) to 150 °C (provided by low-grade industrial steam).

The most suitable hydride-forming materials which satisfy these requirements are AB₅-type intermetallics based on LaNi₅ where Ni is substituted with elements (Al, Mn, Co, etc.), increasing the thermal stability of the intermetallic hydride as compared to LaNi₅H_x. Such intermetallics can be easily activated, and their H sorption characteristics are less sensitive to the impurities in H₂ (first of all, water vapors) than the Ti-based AB- and AB₂-type hydrogen storage alloys [7]. The influence of various substituting elements in LaNi_{5-x}M_x intermetallics on their structural, thermodynamic, magnetic, and hydrogen sorption properties has been analyzed by Joubert et al. in their review [8]. The substitution of Ni with Al [8–10] and Mn [11] has the strongest effect on the increase in the stability of the intermetallic hydrides. Multicomponent AB₅-type alloys (A – La or La + Ce; B – Ni, Co, Al, and Mn) were shown to exhibit H₂ plateau pressures at ambient temperature far below 1 atm and to compress H₂ to 5–10 atm when heated to 150–170 °C [12,13].

Apart from thermodynamic constraints specifying the values of P_{eq} to be below H₂ charge pressure, P_L ≈ 1 atm, at the cooling temperature, T_L ≈ 15–20 °C, and above H₂ discharge pressure, P_H ≈ 2–5 atm, at the heating temperature, T_H ≈ 90–150 °C, high rates of H₂ uptake and release should also be provided on both the material and system level. Considering the limited pressure driving force when absorbing near-atmospheric pressure H₂, the acceleration of this process is the most critical problem. On the material level, it relates to the improvement in hydrogenation kinetics, while the improvement in H₂ uptake dynamics in the system mainly depends on the augmentation of heat exchange between the MH material and the cooling means of the MH reactor.

The improvement in hydrogenation kinetics, along with facilitating activation and adding poisoning tolerance, can be achieved by introducing catalysts of the dissociative H₂ chemisorption, including Pd or Pd–Ni nanoparticles deposited onto the AB₅ substrate [14]. The less expensive but still efficient approach is the creation of MH-based composites containing minor additives of graphene-like material with deposited Ni nanoparticles (Ni/GLM). Apart from catalyzing hydrogenation reactions, such composites are characterized by improved effective thermal conductivity (ETC), thus assisting in the acceleration of the H₂ charge dynamics of the MH reactor [15]. Alternatively, ETC can be increased by adding expanded natural graphite (ENG) to the MH material [16].

Finally, the thermal augmentation methods include optimising the size and geometry of the MH reactors. The most frequently used methods combine the increase in (1) ETC (e.g., by using ENG), (2) heat transfer surface area (finned or coiled heat exchangers), and (3) the overall heat transfer coefficient (internal heat exchanger + external cooling jacket) [17].

This work presents results of the activities of the authors representing FRC PCP&MC RAS (Russia) and HySA Systems (South Africa) on the development of systems which can absorb low-pressure H₂ and to further desorb it at higher pressures. The studies of the Russian team aimed toward the development of MH H₂ storage and supply unit fed by H₂ from a solid oxide electrolyzer were focused on the use of LaNi_{5-x}Al_x intermetallics with Ni/GLM additives. The activities of the HySA Systems team in South Africa were focused on the development of an MH hydrogen compression unit with suction pressure below 1 atm comprising a powder mixture of a multi-component AB₅-type battery alloy with ENG additives loaded into a standard HySA Systems MH container for medium-pressure hydrogen compression [4].

2. Results

2.1. MH Materials

The analysis of data in the literature [8–10] and our own preliminary results on hydrogen absorption in aluminium-substituted LaNi₅ at P(H₂) = 1 atm and T = 20–40 °C

(Figure 1) shows that the maximum hydrogen absorption capacity can be achieved when the content of aluminium in $\text{LaNi}_{5-x}\text{Al}_x$ corresponds to $x = 0.55$. At the lower x values, when P_{eq} in the plateau region of the pressure–composition isotherm approaches 1 atm, the capacity drop, especially pronounced when increasing the absorption temperature, is observed. A further increase in x results in reducing the H absorption capacity that is typical for the Al-substituted alloys, despite significant decreases in the plateau pressures in H– $\text{LaNi}_{5-x}\text{Al}_x$ systems when increasing x [8]. In addition, hydrogen desorption from the hydrogenated alloys $\text{LaNi}_{5-x}\text{Al}_x$ ($x > 0.55$) at moderate (<100 °C) temperatures is characterized by lower plateau pressures resulting in high residual H concentrations and, in turn, low reversible H sorption capacities at the operating conditions.

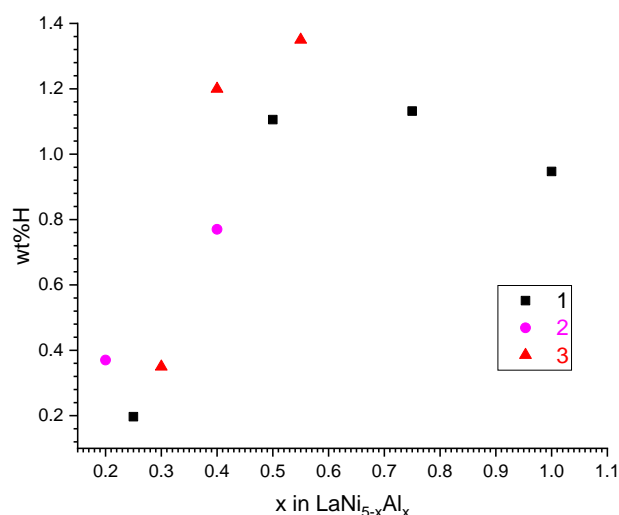


Figure 1. Hydrogen absorption capacity of $\text{LaNi}_{5-x}\text{Al}_x$ intermetallics at $P(\text{H}_2) = 1$ atm. 1—[10], $T = 40$ °C; 2—[9], $T = 20$ °C; 3—this work, $T = 20$ °C.

The $\text{LaNi}_{4.45}\text{Al}_{0.55}$ alloy was prepared in an upscaled ($\times 10$ kg) amount and used in further studies by the Russian co-authors of this work.

In the studies carried out by HySA Systems in South Africa, a multi-component AB_5 -type alloy was used. According to the results of EDX analysis (see Supplementary Information; Figure S1 and Table S1), the composition of the used alloy corresponded to the formula $\text{La}_{0.41}\text{Ce}_{0.59}\text{Ni}_{3.71}\text{Co}_{0.52}\text{Mn}_{0.36}\text{Al}_{0.29}$ ($B/A = 4.88$).

XRD analysis of the as-delivered and hydrogenated alloys confirmed that each sample contains a single phase of CaCu_5 -type intermetallic (intermetallic hydride), space group $P6/mmm/\#191$ (Figure S2 and Table S2). Rietveld refinement of the XRD patterns yielded acceptable residuals when R_p values varied between 3.1 and 5.4%, except for the starting $\text{LaNi}_{4.45}\text{Al}_{0.55}$ alloy ($R_p = 13.6\%$), which exhibited a bigger crystallite size and noticeable preferred orientation in the (1 0 0) plane (Table S2).

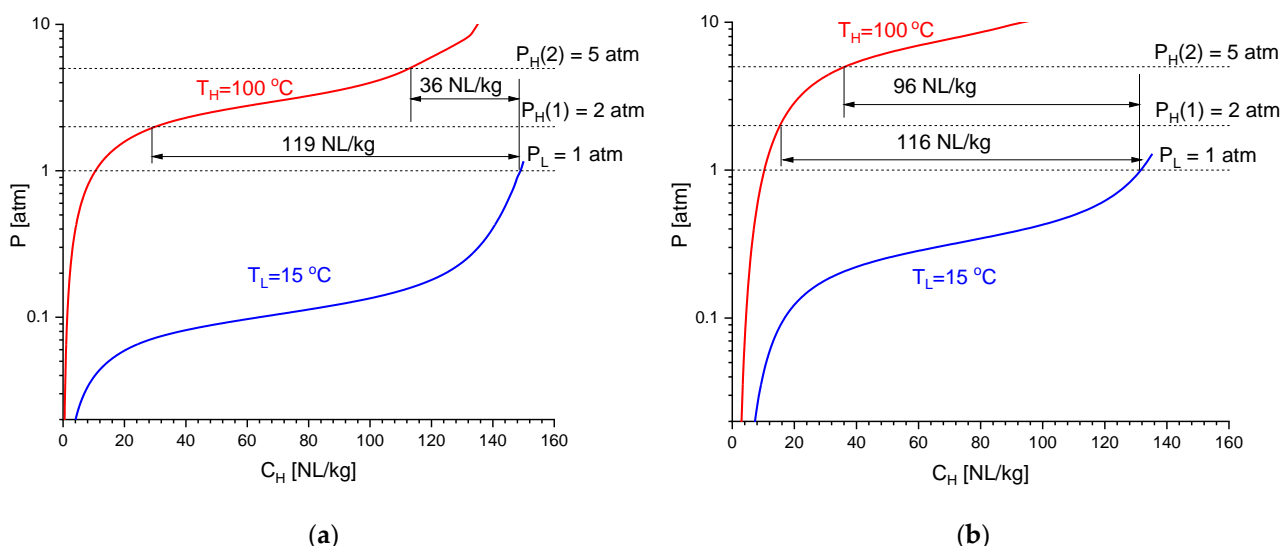
The data on lattice periods and unit cell volumes calculated from the results of Rietveld refinement of the XRD patterns are summarized in Table 1. The lattice periods and unit cell volume of $\text{LaNi}_{4.45}\text{Al}_{0.55}$ are in good correspondence with the reference data for $\text{LaNi}_{4.5}\text{Al}_{0.5}$: $a = 5.03$ Å, $c = 4.03$ Å, $c/a = 0.80$, $V = 88.3$ Å³ [18]. At the same time, the multi-component AB_5 intermetallic studied in this work exhibits a unit cell volume 1.6–2.4% lower than the values reported in [19,20] for the battery alloys of similar compositions but containing La-rich mischmetal (~ 70 at.% La) as an A-component. The reason for the deviation appears to be the higher content of cerium (atomic radius 185 pm) in our case, while the intermetallics studied in [19,20] contained more lanthanum, characterized by a bigger atomic radius (195 pm).

Table 1. Lattice periods and unit cell volumes of the studied samples calculated from Rietveld refinement of their XRD patterns.

| Sample | | a [Å] | c [Å] | c/a | V [Å ³] | $\Delta V/V_0$ [%] |
|---|---------|-------------|-------------|-------|-----------------------|--------------------|
| LaNi _{4.45} Al _{0.55} | Alloy | 5.0355 (1) | 4.0230 (1) | 0.80 | 88.344 (4) | 16.37 |
| | Hydride | 5.3302 (2) | 4.1783 (3) | 0.78 | 102.808 (8) | |
| La _{0.41} Ce _{0.59} Ni _{3.71} Co _{0.52} Mn _{0.36} Al _{0.29} | Alloy | 4.97948 (4) | 4.05629 (6) | 0.81 | 87.102 (2) | 21.08 |
| | Hydride | 5.34975 (8) | 4.2550 (1) | 0.80 | 105.462 (3) | |

Both alloys were found to exhibit reproducible hydrogen absorption/desorption performances after 1 h long evacuation at $T = 90$ °C followed by exposure in hydrogen at $P = 5$ atm, cooling to ambient temperature and being kept under H₂ pressure for 5–6 h.

Figure 2 presents isotherms of hydrogen absorption and desorption for the studied intermetallics. For the correct comparison, the experimental PCT data taken for LaNi_{4.45}Al_{0.55} (20–90 °C; 0.04–15 atm) and La_{0.41}Ce_{0.59}Ni_{3.71}Co_{0.52}Mn_{0.36}Al_{0.29} (20–120 °C, 0.02–30 atm) were processed using the model of phase equilibria in hydrogen–metal systems [21], and the absorption ($T_L = 15$ °C) and desorption ($T_H = 100$ °C) isotherms shown in Figure 2 were calculated using the refined fitting parameters.

**Figure 2.** Calculated isotherms of H₂ absorption at $T_L = 15$ °C and H₂ desorption at $T_H = 100$ °C for the low-pressure AB₅-type intermetallics LaNi_{4.45}Al_{0.55} (a) and La_{0.41}Ce_{0.59}Ni_{3.71}Co_{0.52}Mn_{0.36}Al_{0.29} (b).

As it can be seen, both intermetallics exhibit similar reversible hydrogen sorption capacities: 116–119 NL/kg (1.03–1.05 wt.% H) when operating in the range of $T_L = 15$ °C/ $P_L = 1$ atm – $T_H = 100$ °C/ $P_H = 2$ atm. However, due to the slightly lower thermal stability of La_{0.41}Ce_{0.59}Ni_{3.71}Co_{0.52}Mn_{0.36}Al_{0.29} hydride (the fitted values of hydrogenation entropy and enthalpy correspond to $\Delta S^\circ = -112.20 \pm 0.01$ J/(mol H₂ K) and $\Delta H^\circ = -35.615 \pm 0.004$ kJ/mol H₂) as compared to LaNi_{4.45}Al_{0.55}H_x ($\Delta S^\circ = -108.22 \pm 0.02$ J/(mol H₂ K); $\Delta H^\circ = -36.90 \pm 0.02$ kJ/mol H₂), the latter exhibits a significant drop (by 3.3 times) in the reversible capacity when the discharge pressure increases to $P_H = 5$ bar, while for the multi-component AB₅-type alloy, the capacity remains close to 100 NL/kg (0.85 wt.% H). Apparently, low errors of the refined values of ΔS° and ΔH° are related to the specifics of the modeling procedure [21], which assumes the error of the refined fitting parameter to be equal to its biggest increment (decrement), which results in the 1% increase in the sum of the squared shortest distances of the experimental points from the calculated PCI curves built in coordinates $C/C_{\max} - \ln P$.

Thus, we recommend using $\text{LaNi}_{4.45}\text{Al}_{0.55}$ for buffer hydrogen storage in systems characterized by near-atmospheric pressures of the produced H_2 and relatively low (up to 1 atm gage) pressures of H_2 consumption typical for the renewable energy systems based on reversible solid oxide fuel cells [1]. The $\text{La}_{0.41}\text{Ce}_{0.59}\text{Ni}_{3.71}\text{Co}_{0.52}\text{Mn}_{0.36}\text{Al}_{0.29}$ alloy can be used as a material for the first stage of a thermally driven MH H_2 compressor with a near-atmospheric suction pressure for the utilization of low-pressure H_2 .

2.2. System Development

2.2.1. MH Hydrogen Storage Unit Charged from Solid Oxide Electrolyzer

The low-pressure hydrogen storage unit developed by FRC PCP&MC RAS (Figure 3) comprises a stainless-steel cylindrical container (1) equipped with an inner heat exchanger (2) made as a double-circuit coiled copper tubing, and an outer heating/cooling jacket (3). The containment ends are closed by two flanges (4,5). The top flange (4) carries a H_2 inlet/outlet port (4.1) connected to tubular filter (4.2), as well as ports (4.3) for the input and output of cooling/heating fluid (cold and hot water), a connector for the pressure sensor (4.4), and a thermocouple probe (4.5) for measuring the temperature of the MH bed. The inner space of the containment (1), 20 mm in the diameter and 290 mm in the height, was filled with 8.5 kg of $\text{LaNi}_{4.45}\text{Al}_{0.55}$ powder mixed with 100 g (1.16 wt.%) of Ni/GLM powder for the improvement in hydrogen absorption kinetics and the increase in the effective thermal conductivity of the MH bed [15].

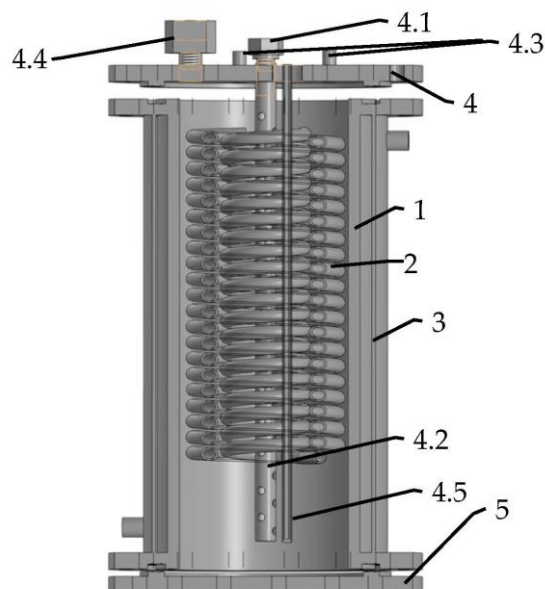


Figure 3. Layout of hydrogen storage unit developed at FRC PCP&MC RAS. 1—cylindrical containment; 2—heat exchanger; 3—heating/cooling jacket; 4—top flange: 4.1— H_2 inlet/outlet port, 4.2—tubular filter, 4.3—heating/cooling ports, 4.4—connector for pressure sensor, 4.5—thermocouple probe; 5—bottom flange.

The developed unit exhibited the maximum hydrogen absorption capacity of 1200 NL, of which, about 1000 NL was absorbed at $P(\text{H}_2) \leq 1$ atm when cooled to 15–20 °C with running water. The amount of hydrogen further desorbed at $P(\text{H}_2) \geq 2$ atm during water heating to 70–90 °C exceeded 900 NL, which corresponds to 100 NL/kg, or ~84% of the theoretical (equilibrium) reversible H storage capacity of $\text{LaNi}_{4.45}\text{Al}_{0.55}$ in the range of operating temperatures and pressures 15–100 °C and 1–2 atm, respectively (see Figure 2a). The unit was successfully tested in integration with a solid oxide electrolyzer.

2.2.2. MH Unit for Low-Pressure Hydrogen Compression

As mentioned above, the low-pressure H₂ compression unit developed by HySA Systems used a standard MH container for medium-pressure hydrogen compression, described in ref. [4]. The cylindrical stainless-steel container (625 mm long and 2.68 dm³ in the inner volume) with an inner heat exchanger (finned tube) and an outer heating/cooling jacket was filled with 8.3 kg of the powdered mixture of La_{0.41}Ce_{0.59}Ni_{3.71}Co_{0.52}Mn_{0.36}Al_{0.29} with 1wt.% of ENG.

Figure 4 schematically shows the connection of the MH container to the testrig. During the tests, hydrogen pressure was measured both at the front (H₂ supply/removal pipeline; P(front)) and back (P(back)) sides of the container using a two-channel absolute/differential PD39 pressure sensor (0–10 atm absolute). For the connection of the rear side of the container to the pressure sensor, as well as for the input of a thermocouple measuring the temperature in the MH bed, the MH loading port of the container was used. Additionally, the mass flow rate (FR) of hydrogen supplied to or released from the MH container was measured. The temperatures of the supplied (T(in)) and drained (T(out)) cooling/heating fluid (water/steam), along with the MH bed temperature (T(MH)) in the container, close to its back side, were measured as well.

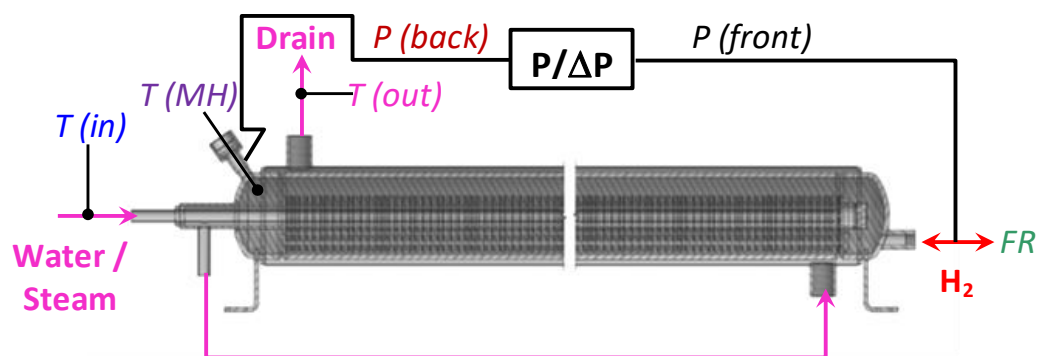


Figure 4. Schematics of the tests of MH container for the low-pressure H₂ compression. T(in)—steam (water) inlet temperature, T(out)—steam (water) outlet temperature, T(MH)—temperature in the MH bed, P/ΔP—absolute/differential pressure sensor, P(front)—H₂ pressure at the input/output of the MH container, P(back)—H₂ pressure from the opposite side, FR—mass flow rate of the absorbed/desorbed H₂.

The results of the tests (see Figure 5) showed that the total hydrogen capacity of the MH container exceeded 1000 NL, of which, about 850 NL was absorbed at the pressure below 1 atm during the cooling of the container with running water at T = 16–18 °C. About 80% of the low-pressure hydrogen (670 NL) was absorbed in 30 min with a maximum flow rate of 30 NL/min. The MH temperature increased to ~75 °C almost immediately after the start of the low-pressure H₂ supply, and the pressure drop between the entrance to the container, P(front), and its rear side, P(back), did not exceed 0.05 atm. Further heating of the container by steam (T~120 °C) resulted in the desorption of hydrogen at higher pressures; in doing so, about 650 NL H₂ was desorbed from the container at a pressure above 5 atm and a flow rate of 10–30 NL/min.

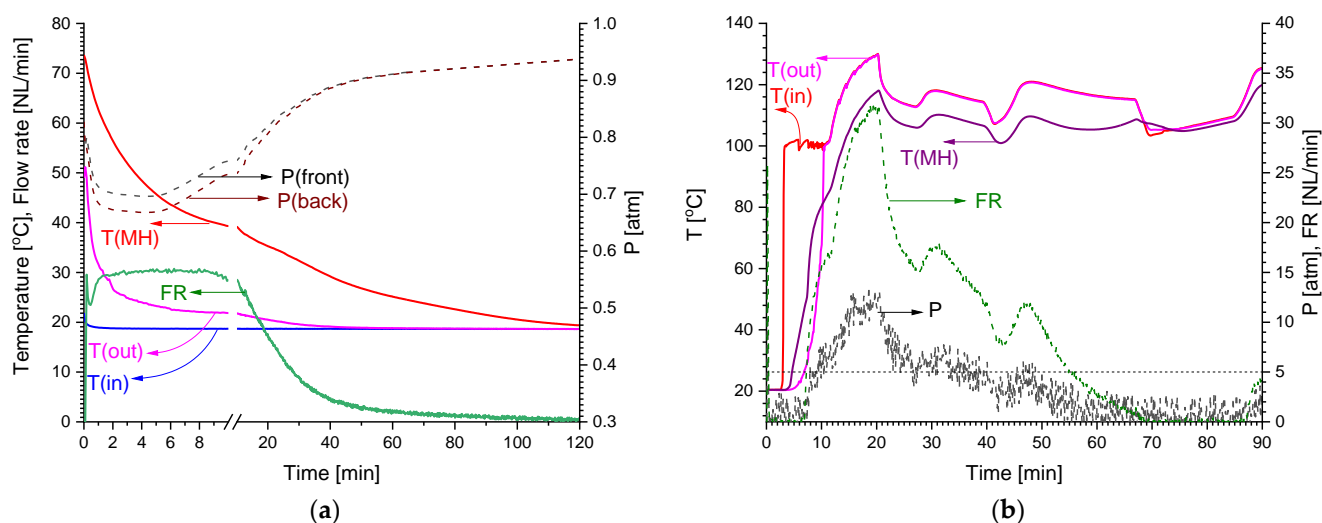


Figure 5. Results of tests of MH container for low-pressure H₂ compression: H₂ absorption (a) and H₂ desorption (b).

3. Discussion

Figure 6 compares the H₂ charge dynamic performance of the low-pressure hydrogen storage unit developed at FRC PCP&MC RAS (1) and the unit for the low-pressure H₂ compression developed by HySA Systems (2). Both units can absorb hydrogen supplied below atmospheric pressure; the hydrogen absorption capacity achieved after 2 h long operation was about 90% of the maximum one observed after the charge at $P(\text{H}_2) = 5$ atm and ambient temperature. In doing so, the average H absorption rate exceeded 10 NL/min for the MH load between 8.3 and 8.6 kg, which corresponded to the specific rate of more than 1.15–1.20 NL/(min kg). This shows the technical feasibility of charging MH units with near-atmospheric-pressure hydrogen with reasonable productivity when the absorption plateau pressure of the used AB₅-type MH material is about 0.1–0.3 atm (Figure 2).

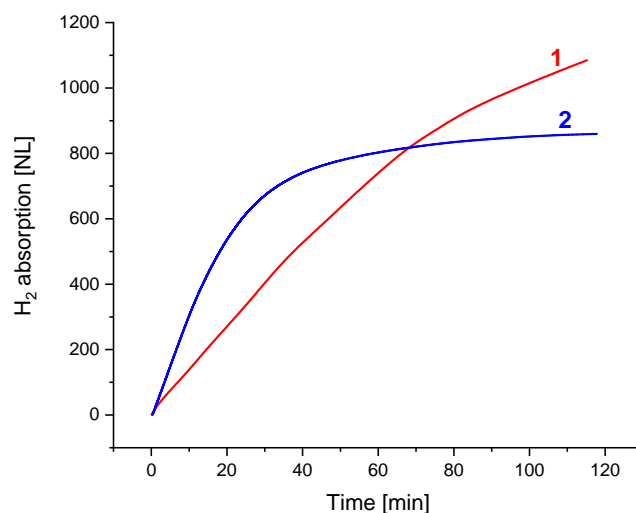


Figure 6. Dynamics of H₂ charge of the MH hydrogen storage (1: FRC PCP&MC RAS) and compression (2: HySA Systems) units at the pressure of the feed H₂ below 1 atm (absolute).

Slower H₂ charge dynamics of the FRC PCP&MC RAS unit (1), first of all, are caused by the lower efficiency of the used inner heat exchanger (coiled tube) as compared to the HySA Systems unit (2), in which the heat exchanger was made as a finned tube with fin pitch of 5 mm. However, the advantage of the former unit is the almost constant hydrogen absorption flow rate throughout the operation period, which improves the overall system

performance when operating in the integration with the solid oxide electrolyzer. The further heating of the unit to a moderate temperature, 70–90 °C, would allow hydrogen to be released at $P \geq 2$ atm, which is sufficient for H₂ supply to a solid oxide fuel cell stack, for example, when the SOC unit is used in the reversible “electrolyzer–fuel cell” mode.

The analysis of the low-pressure hydrogen compression performance of the HySA Systems unit (2; see also Figure 5) allows us to conclude that the productivity of hydrogen compression from $P_L = 1$ atm ($T_L = 15$ °C) to $P_H = 5$ atm ($T_H = 120$ °C) at the typical duration of an absorption–desorption cycle of 50–60 min [22] can achieve ~ 0.1 Nm³/h per 1 kg of the used multi-component AB₅-type alloy. A further increase in hydrogen compression productivity can be achieved by optimising the MH material, first of all, towards the acceleration of hydrogen absorption kinetics at a low pressure driving force. The replacement of the ENG additive with Ni/GLM, along with the optimization of its content in the composite [15], can be promising in solving this problem.

4. Materials and Methods

The laboratory samples of LaNi_{5-x}Al_x intermetallics ($x = 0.2$ – 0.8) used in preliminary studies were prepared via arc melting of the components (La–98%; Ni, Al–99.5+%) under purified argon; the ingots were turned over and re-melted 3 times. The LaNi_{4.45}Al_{0.55} alloy for further studies and use in the low-pressure MH hydrogen storage unit was prepared via induction melting in an alumina crucible under an argon atmosphere. All the alloys were studied in as-cast forms; no heat treatments were applied.

The Ni/GLM material was prepared via the reduction of a freeze-dried suspension of graphite oxide in Ni(CH₃COO)₂ aqueous solution in hydrogen flow at $T = 300$ – 500 °C; further details are presented in Ref. [23]. The LaNi_{4.45}Al_{0.55}–Ni/GLM composite was prepared by mixing the powders of the components (8.5 kg and 100 g, respectively).

The multi-component AB₅-type alloy used in HySA Systems studies was supplied in $\times 10$ kg amount by Guangdong Provincial Key Laboratory of Rare Earth Development and Application (Guangzhou, China). The composition of a standard battery alloy was modified by the supplier, in consultation with HySA Systems, to provide the desired H₂ absorption/desorption performance: minimum H₂ absorption plateau pressure (below 1 atm) at near-ambient temperature and maximum H₂ desorption plateau pressure (above 2 atm) at the temperatures above 70–90 °C.

The expanded natural graphite (ENG) was prepared via the heating of graphite oxide powder (KP50 expandable graphite, Bolun Industrial Limited/Huaian, China; 500 μ , 99.9+%) to 900 °C in an open tube furnace for 1 h. The powders of 8.3 kg of La_{0.41}Ce_{0.59}Ni_{3.71}Co_{0.52}Mn_{0.36}Al_{0.29} alloy and 83 g of ENG were mixed and loaded into the MH container for low-pressure H₂ compression.

XRD studies were carried out using Thermo Scientific (Waltham, MA, USA) ARL X'TRA (FRC PCP&MC RAS) and Rigaku Miniflex 600 (HySA Systems), Tokyo, Japan, instruments, using Cu-K α radiation, in the range of Bragg angles $2\theta = 20$ – 90° . The hydrogenated samples taken for the XRD measurements were stabilized via exposure to carbon monoxide (FRC PCP&MC RAS) or ambient air at liquid nitrogen temperature (HySA Systems). A standard α -Al₂O₃ sample was used for the determination of the instrumental contribution into peak profile parameters. The XRD patterns were processed via Rietveld analysis using GSAS software (2001 release, last update in 2009). During the refinements, the Gaussian profile parameters (GU, GV, and GW) were fixed (kept the same as for the Al₂O₃ standard), and only two Lorentzian profile parameters were refined: LX (size broadening) and LY (strain broadening).

EDX analysis of the multi-component AB₅-type alloy was carried out using a Zeiss Auriga scanning electron microscope (Zeiss, Oberkochen, Germany); imaging in secondary electrons was carried out at the acceleration voltage of 15–20 kV.

Hydrogen absorption/desorption PCT studies were carried out using Sieverts setups in the range of temperatures of 20–120 °C and pressures of 0.01–40 atm, with a sample weight of 1–2 g, a sample holder volume of 12 cm³, and the reference volume, depending

on the instrument used, being from 12 to 35 cm³. The as-collected PCT data were processed using the model of phase equilibria in hydrogen–metal systems [21]; the average fitting error corresponded to $\Delta C/C_{\max}$ below 0.06%.

Testing of the developed units was carried out using in-house built testtrigs, allowing us to monitor the H₂ charge/discharge flow rates, hydrogen pressures, and temperatures.

5. Conclusions

This work has shown the technical feasibility of the storage and thermally driven compression of low-pressure (1 atm absolute) hydrogen with a compression ratio from 2 to 5 in the temperature range from 15 to 20 to 70 to 120 °C by using AB₅-type hydride-forming intermetallics characterized by plateau pressures of 0.1–0.3 atm at the ambient temperature and 3–8 atm at T = 100 °C. The use of powdered mixtures of these alloys with minor additives of the reduced graphite oxide (expanded natural graphite) or graphene-like material with deposited nickel nanoparticles allowed us to achieve the rate of hydrogen uptake and release above 10 NL/min for the 1 Nm³ H₂ capacity unit, or above 1.2 NL/min per 1 kg of the used material.

6. Patents

The following patented solutions contributed to the results reported in this work:

- Metal hydride bed, metal hydride container, and method for the making thereof, by M. Lototsky, M.W. Davids, B.G. Pollet, V.M. Linkov and Y. Klochko. WO 2015/189758 A1 (2015).
- Nickel-graphene hydrogenation catalyst and method of its production, by A.A. Arbutov, S.A. Mozhzhukhin, A.A. Volodin, P.V. Fursikov and B.P. Tarasov. RU 2660232 C1 (2018).
- Low-pressure hydrogen accumulator of multiple action, by B.P. Tarasov, A.A. Arbutov, S.A. Mozhzhukhin, A.A. Volodin, P.V. Fursikov and M.V. Lototsky. Application RU2023108442 (2023).

Supplementary Materials: The following supporting information can be downloaded at: <https://www.mdpi.com/article/10.3390/inorganics11070290/s1>, Figure S1: Energy dispersion spectrum and low-magnification SEM image of the multi-component AB₅-type alloy; Table S1: Summary of EDX analysis of the multi-component AB₅-type alloy; Figure S2: Refined XRD patterns of the studied samples; Table S2: Summary of Rietveld refinement of XRD patterns of the studied samples.

Author Contributions: Conceptualization, B.T. and M.L.; methodology, A.A. and M.L.; validation, S.M., M.W.D. and J.A.; formal analysis, A.V. and P.F.; investigation, B.T., A.A. and M.L.; resources, A.A. and M.W.D.; writing and visualization, M.L. and B.T.; supervision, B.T. and A.A.; project administration and funding acquisition, B.T. and M.L. All authors have read and agreed to the published version of the manuscript.

Funding: This research was funded by the Russian Ministry of Science and Higher Education (Agreement No. 075-15-2022-1126) and the Department of Science and Innovation of South Africa (HySA Program, Key Project KP6-S02).

Data Availability Statement: The data presented in this study are available on request from the corresponding author.

Acknowledgments: This work was performed using the equipment of FRC PCP&MC RAS, <https://www.icp.ac.ru/en/>, and HySA Systems hosted by the University of the Western Cape, <http://hysasystems.com/>.

Conflicts of Interest: The authors declare no conflict of interest.

References

1. Brisse, A.; Schefold, J.; Léon, A. High-Temperature Steam Electrolysis. In *Electrochemical Power Sources: Fundamentals, Systems, and Applications*; Elsevier: Amsterdam, The Netherlands, 2022; pp. 229–280.
2. Lee, D.-Y.; Elgowainy, A.; Dai, Q. Life Cycle Greenhouse Gas Emissions of Hydrogen Fuel Production from Chlor-Alkali Processes in the United States. *Appl. Energy* **2018**, *217*, 467–479. [[CrossRef](#)]
3. Sdanghi, G.; Maranzana, G.; Celzard, A.; Fierro, V. Review of the Current Technologies and Performances of Hydrogen Compression for Stationary and Automotive Applications. *Renew. Sustain. Energy Rev.* **2019**, *102*, 150–170. [[CrossRef](#)]
4. Lototsky, M.; Linkov, V. Thermally Driven Hydrogen Compression Using Metal Hydrides. *Int. J. Energy Res.* **2022**, *46*, 22049–22069. [[CrossRef](#)]
5. Cuevas, F.; Latroche, M. Intermetallic Alloys as Hydrogen Getters. *J. Alloys Compd.* **2022**, *905*, 164173. [[CrossRef](#)]
6. Lototsky, M.V.; Yartys, V.A.; Klochko, Y.V.; Borisko, V.N.; Starovoitov, R.I.; Azhazha, V.M.; V'yugov, P.N. Applications of Zr-V Hydrogen Getters in Vacuum-Plasma Devices: Phase-Structural and Hydrogen Sorption Characteristics. *J. Alloys Compd.* **2005**, *404*, 724–727. [[CrossRef](#)]
7. Sandrock, G. A Panoramic Overview of Hydrogen Storage Alloys from a Gas Reaction Point of View. *J. Alloys Compd.* **1999**, *293*, 877–888. [[CrossRef](#)]
8. Joubert, J.-M.; Paul-Boncour, V.; Cuevas, F.; Zhang, J.; Latroche, M. LaNi₅ Related AB₅ Compounds: Structure, Properties and Applications. *J. Alloys Compd.* **2021**, *862*, 158163. [[CrossRef](#)]
9. Dashbabu, D.; Kumar, E.A.; Jain, I.P. Thermodynamic Analysis of a Metal Hydride Hydrogen Compressor with Aluminium Substituted LaNi₅ Hydrides. *Int. J. Hydrogen Energy* **2022**. [[CrossRef](#)]
10. Diaz, H.; Percheron Guegan, A.; Achard, J.; Chatillon, C.; Mathieu, J. Thermodynamic and Structural Properties of LaNi_{5-y}Al_y Compounds and Their Related Hydrides. *Int. J. Hydrogen Energy* **1979**, *4*, 445–454. [[CrossRef](#)]
11. Chen, X.; Xu, J.; Zhang, W.; Zhu, S.; Zhang, N.; Ke, D.; Liu, J.; Yan, K.; Cheng, H. Effect of Mn on the Long-Term Cycling Performance of AB₅-Type Hydrogen Storage Alloy. *Int. J. Hydrogen Energy* **2021**, *46*, 21973–21983. [[CrossRef](#)]
12. Lv, L.; Lin, J.; Yang, G.; Ma, Z.; Xu, L.; He, X.; Han, X.; Liu, W. Hydrogen Storage Performance of LaNi_{3.95}Al_{0.75}Co_{0.3} Alloy with Different Preparation Methods. *Prog. Nat. Sci. Mater. Int.* **2022**, *32*, 206–214. [[CrossRef](#)]
13. Lototsky, M.V.; Yartys, V.A.; Tarasov, B.P.; Davids, M.W.; Denys, R.V.; Tai, S. Modelling of Metal Hydride Hydrogen Compressors from Thermodynamics of Hydrogen—Metal Interactions Viewpoint: Part I. Assessment of the Performance of Metal Hydride Materials. *Int. J. Hydrogen Energy* **2021**, *46*, 2330–2338. [[CrossRef](#)]
14. Lototsky, M.V.; Williams, M.; Yartys, V.A.; Klochko, Y.V.; Linkov, V.M. Surface-Modified Advanced Hydrogen Storage Alloys for Hydrogen Separation and Purification. *J. Alloys Compd.* **2011**, *509*, S555–S561. [[CrossRef](#)]
15. Tarasov, B.P.; Arbuzov, A.A.; Volodin, A.A.; Fursikov, P.V.; Mozhzhuhin, S.A.; Lototsky, M.V.; Yartys, V.A. Metal Hydride—Graphene Composites for Hydrogen Based Energy Storage. *J. Alloys Compd.* **2022**, *896*, 162881. [[CrossRef](#)]
16. Atalmis, G.; Sattarkhanov, K.; Demiralp, M.; Kaplan, Y. The Effect of Expanded Natural Graphite Added at Different Ratios of Metal Hydride on Hydrogen Storage Amount and Reaction Kinetics. *Int. J. Hydrogen Energy* **2023**. [[CrossRef](#)]
17. Sreeraj, R.; Aadhithyan, A.K.; Anbarasu, S. Integration of Thermal Augmentation Methods in Hydride Beds for Metal Hydride Based Hydrogen Storage Systems: Review and Recommendation. *J. Energy Storage* **2022**, *52*, 105039. [[CrossRef](#)]
18. Kodama, T. The Thermodynamic Parameters for the LaNi_{5-x}Al_x-H₂ and MmNi_{5-x}Al_x-H₂ Systems. *J. Alloys Compd.* **1999**, *289*, 207–212. [[CrossRef](#)]
19. Vivet, S.; Joubert, J.-M.; Knosp, B.; Percheron-Guégan, A. Effects of Cobalt Replacement by Nickel, Manganese, Aluminium and Iron on the Crystallographic and Electrochemical Properties of AB₅-Type Alloys. *J. Alloys Compd.* **2003**, *356*, 779–783. [[CrossRef](#)]
20. Ma, J. Effect of Heat Treatment on the Microstructure and Electrochemical Properties of AB₅-Type MiNi_{3.60}Co_{0.85}Mn_{0.40}Al_{0.15} Hydride Alloy: 1. The Microstructure and P-C Isotherms. *Int. J. Hydrogen Energy* **2002**, *27*, 57–62. [[CrossRef](#)]
21. Lototsky, M.V. New Model of Phase Equilibria in Metal—Hydrogen Systems: Features and Software. *Int. J. Hydrogen Energy* **2016**, *41*, 2739–2761. [[CrossRef](#)]
22. Lototsky, M.V.; Yartys, V.A.; Tarasov, B.P.; Denys, R.V.; Eriksen, J.; Bocharnikov, M.S.; Tai, S.; Linkov, V. Modelling of Metal Hydride Hydrogen Compressors from Thermodynamics of Hydrogen—Metal Interactions Viewpoint: Part II. Assessment of the Performance of Metal Hydride Compressors. *Int. J. Hydrogen Energy* **2021**, *46*, 2339–2350. [[CrossRef](#)]
23. Tarasov, B.P.; Arbuzov, A.A.; Mozhzhuhin, S.A.; Volodin, A.A.; Fursikov, P.V. Composite Materials with 2D Graphene Structures: Applications for Hydrogen Energetics and Catalysis with Hydrogen Participation. *J. Struct. Chem.* **2018**, *59*, 830–838. [[CrossRef](#)]

Disclaimer/Publisher's Note: The statements, opinions and data contained in all publications are solely those of the individual author(s) and contributor(s) and not of MDPI and/or the editor(s). MDPI and/or the editor(s) disclaim responsibility for any injury to people or property resulting from any ideas, methods, instructions or products referred to in the content.